Iran J Earth Sci., 2026; 18(2): 176-190

Iranian Journal of Earth Sciences (IJES)

https://doi.org/10.57647/j.ijes.2025.16907

Research Article

The Shortening and Strain Partitioning in the Southern Kerman-Behabad Coal Field Revealed by Fold Analyses

Yadollh Pourahmadi Toghrolgerdi[1], Mohsen Pourkermani[1]*, Amir Shafiei Bafti[2], Soheila Bouzari[1], Ali Elahi[3]

[1]*Department of Geology, North Tehran Branch, Islamic Azad University, Tehran, Iran*
[2]*Department of Geology, Zarand Branch, Islamic Azad University, Zarand, Iran*
[3]*Department of Mining Engineering, Higher Education Complex of Zarand Shahid Bahonar University of Kerman, Kerman, Iran*

***Corresponding author:** Mohsen.pourkermani@gmail.com

Article History:

Received:
26 July 2024

Revised:
7 October 2024

Accepted:
19 December 2024

Published online:
11 June 2025

Published in Issue:
30 June 2026

Abstract

This paper discusses shortening and strain in folds, highlighting the structural variation in the southern Kerman coal field. In this tectonically active region, the stress resulting from compression and tension in central Iran has largely manifested as folding and faulting, which constitute the major deformation of the area. The research results show compression of the folds in the study area. The results also indicate the complete reversal of the relative ages of ductile and brittle structures, due to faulting that sheared the limbs of most folds in the region. As can be inferred, except for the Kuhbanan and Lekarkoh faults, which existed before the folds and hence played a major role in the area's formation, the remaining faults in the region formed after the folds. In this aspect, the maximum shortening percentage in the area is 70% for the Babnizo fold, and the minimum is 42% for the Eshkli syncline.

Keyword: Kuhbanan, Shortening, Coal Basin, Fold, Lekarkoh

Cite this article: Pourahmadi Toghrolgerdi, Y., Pourkermani, M., Shafiei Bafti, A., Bouzari, S. & Elahi, A., (2026). Iranian Journal of Earth Sciences, The Shortening and Strain Partitioning in the Southern Kerman-Behabad Coal Field Revealed by Fold Analyses, 18(2): 176-190.
https://doi.org/10.57647/ijes.2025.16907

1. Introduction

Iran's current tectonic framework results from the convergence of the Eurasian and Arabian plates (Berberian, 1999, 2001). These movements have primarily affected regions such as the north of Alborz, the northeast of Kopeh Dagh, the southwest and west of Zagros, the northeast strike-slip fault, and the southeast of the Makran structural zones (Fig. 1) (Ezati et al., 2022; Ghanbarian et al., 2022; Rashidi and Derakhshani, 2022; Rashidi et al., 2022; Saccani et al., 2022). This study aims to investigate folds in the southern part of the Kerman coal field, specifically between the Hojedk and Dashtkhak mining areas, to examine strain and folding in the region. Field measurements show some characteristics of these folds, while additional data are estimated from geological mapping and structural analysis. Due to the sequence of sandstone and shale formations in the study area, folded structures have formed on various scales. Given that a comprehensive examination of all these structures within a

1,000 km² area requires an independent study, the present study focuses on the most significant folded structures (technical structures). The study area is located in the northwest of Kerman province and Central Iran, between the cities of Zarand and Dashtkhak. The Zarand-Kuhbanan and Kerman-Raver asphalt roads facilitate access to the area. Numerous public and private coal mines in the region have created a network of asphalted rural roads, providing local access.

2. General geology and tectonics of the study area

Geographic positioning system (GPS) studies demonstrate that Iran's deformation is heterogeneous (Vernant et al., 2004). The closure of several Neotethyan ocean basins during the late Cretaceous and early Tertiary is observed in various parts of Iran, including central Iran (Camp et al., 1982; Tirrul et al., 1983; Jentzer et al., 2020). The study area is located in the northern part of Kerman province, central Iran. From a structural geology perspective, Central and Eastern Iran comprises tectonic blocks separated by major faults such as the Nayband and Kuhbanan faults. Variations in the thickness of the same sedimentary facies (e.g., the Badamo and Seri Dezo limestone formations) may provide evidence for vertical tectonic activity across several blocks of central Iran (Shafii et al., 1998; Dabiri et al., 2017). These blocks, originally separated by small oceanic basins during the Phanerozoic (Berberian and King, 1981; Tirul, 1983), began to close since the middle Tertiary (McCall, 1996). However, many impact zones did not begin to deform until the middle Miocene (Arjmandzadeh et al., 2017; Ait Haddou et al., 2025). The folding of marine sediments younger than 12 million years old in the Iranian plateau suggests that deformation in this area began in the Miocene. This evidence indicates limited extensive deformation of the Iranian plateau over the last 5 million years (Allen et al., 2003; GhasemShirazi et al., 2014). These sediments have played a fundamental role in shaping Iran's current form. Since the Pliocene, the predominant tectonic forces on the Iranian plateau and the surrounding belts have transitioned from compressive to sliding (Tadayon et al., 2017). The tectonic features and seismic data indicate that the area remains tectonically active. The Kerman-Behabad displacement, characterized by minor folds, resulted from the Late Cimmerian orogeny and occurred during the Jurassic-Cretaceous period. This structure evolved alongside sub-structures during the Laramide folding phase and subsequent phases (Artinine and Valanine). However, its effect has diminished due to block displacements and overlapping folding events. The study area is the southern part of the Kerman coal field, which is known as the Kerman-Behabad coal synclinorium (Technoexport, 1969 report). This folded-faulted area is limited to the Urmia-Dokhtar volcanic area from the south, Raver Kalmard heights from the north, Bafgh-Saghand heights from the northwest, and Lekarkoh heights from the east and southeast. Also, the Kuhbanan bedrock fault bounds this syncline to the southwest and the Behabad-Tarz fault to the north. Kerman-Behabad sediments include several geological structures with distinct rock facies and varying ages of formation. These units are briefly discussed below: The first lithological-structural unit comprises folded arkose sandstones and quartz arenite of the Cambrian Iran-Arabian platform, which were deformed during the Katangan orogeny. The outcrop of this unit can also be seen outside the coal basin. The second lithological-structural unit consists of thick sediments from the late Neoproterozoic era to the end of the Upper Jurassic, separated from its underlying and overlying sets by a sharp discontinuity. The Kerman-Behabad floodplain includes many structures with different rock facies and varying ages of formation. The first lithological-structural unit is folded arkose sandstones and quartz arenite. The second lithological-structural unit comprises a series of thick sedimentary units from the late Neoproterozoic to the end of the Upper Jurassic. From a technical point of view, these sub-facies include asymmetric folds with a northwest-southeast strike, affected by transverse folds of later metamorphisms. The third lithological-structural unit includes limestone and conglomerate-sand sediments. In terms of structural style, lithology, and folding mode, the second set can be divided into two subfacies: A) the lower subfacies contains upper Neoproterozoic sediments, Paleozoic, and up to a part of the upper Triassic (Retian), which is generally surrounded by the sediments of the Kerman-Behabad synclinorium. Structurally, these subfacies include asymmetric folds with a northwest-southeast strike, affected by later transverse folds. B) The upper subfacies contains sandstones, shales, and coal layers with Triassic to Lower Jurassic-Cretaceous age. Structurally, this subfacies is similar to its overlying subfacies and shows greater variation due to higher strain. The Kerman coal basin includes a thick sequence of sedimentary formations from the upper Neoproterozoic to the Quaternary, with some local outcrops in geological sections (Fig. 2b). The third lithological-structural unit comprises limestone and conglomerate-sandstone sediments. This unit overlays the folds of the second unit through an angular discontinuity (Fig. 1c). The satellite image of the study area represents the northwest-southeast trend of the folds and the different scales of the folds, varying from a few hundred meters to several kilometers (Fig. 4). Some of these smaller folds have formed due to secondary changes from larger folds. Fig. 4 shows a satellite image of the folds in the study area. Given the presence of dominant resistant and non-resistant

sedimentary sequences (sandstone and shale) in the study area, abundant non-tectonic folds (e.g., gravity and expansion) are found in the region. To our knowledge, these folds have not been analyzed at any scale in the region. Examining the tightness of folds, which represents the amount of tension in the area, is among the most common classifications of folds. The most well-known of these classifications is the one proposed by Fleuty (1964), which is the interdial angle from the hinge region to the ridges. Based on this method, the folds are divided into 7 groups. The study area contains several structures with different rock facies and varying ages of formation. However, two main units dominate the region. The first lithological-structural unit belongs to folded arkose sandstones and quartz arenite. The second lithological-structural unit comprises a series of thick sedimentary units from the late Neoproterozoic to the end of the Upper Jurassic.

3. Structural examination of folds

Table 1 presents the field dimensions of the studied folds. One noteworthy point in this table is the N-S trend of the folds and their varying scales, ranging from a few hundred meters to several kilometers. Some of these smaller folds are secondary and have formed from larger folds due to secondary changes. Notably, non-tectonic folds (e.g., gravity and expansion) are found abundantly in the region due to the dominant resistant and non-resistant sedimentary sequences (sandstone and shale). Yet, these folds have not been studied. In the study area, 17 folding structures were investigated, with their characteristics presented in Table 1.

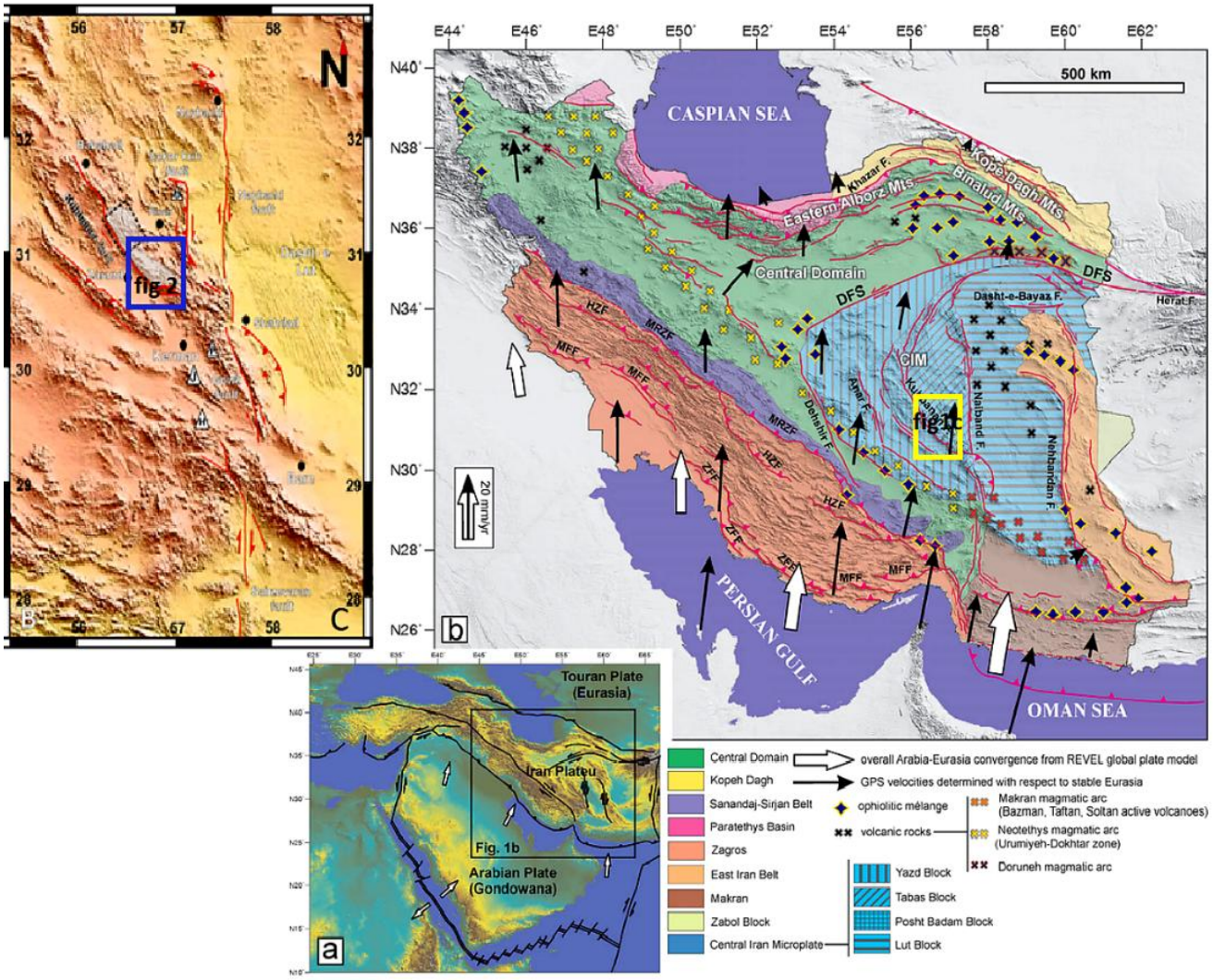

Figure 1. a) Geographical setting of the study area on the convergence direction map (Javadi, 2013); b) Main sedimentary-structural zones of Iran (changed from Aghanabati, 2004) with major faults discussed in the text. White and black arrows are from Sella et al. (2002) and Vernant (2004); c) Elevation view of central and eastern Iran; errors are displayed in red. The convergence of bedrock faults is depicted in the northern part of Kerman. The boundary between the highlands and the plains is the fault, and the highlands are the product of the faulting and folding activities (folded belts-thrust faults). The Kerman coal map, shaded in gray, and the black dashed line denote the study area. The peaks of the mountain ranges are shown with white triangles (D: Darband peak, P: Pelvar peak, J: Jopar peak, and H: Hazar peak)

10.57647/ijes.2025.16907

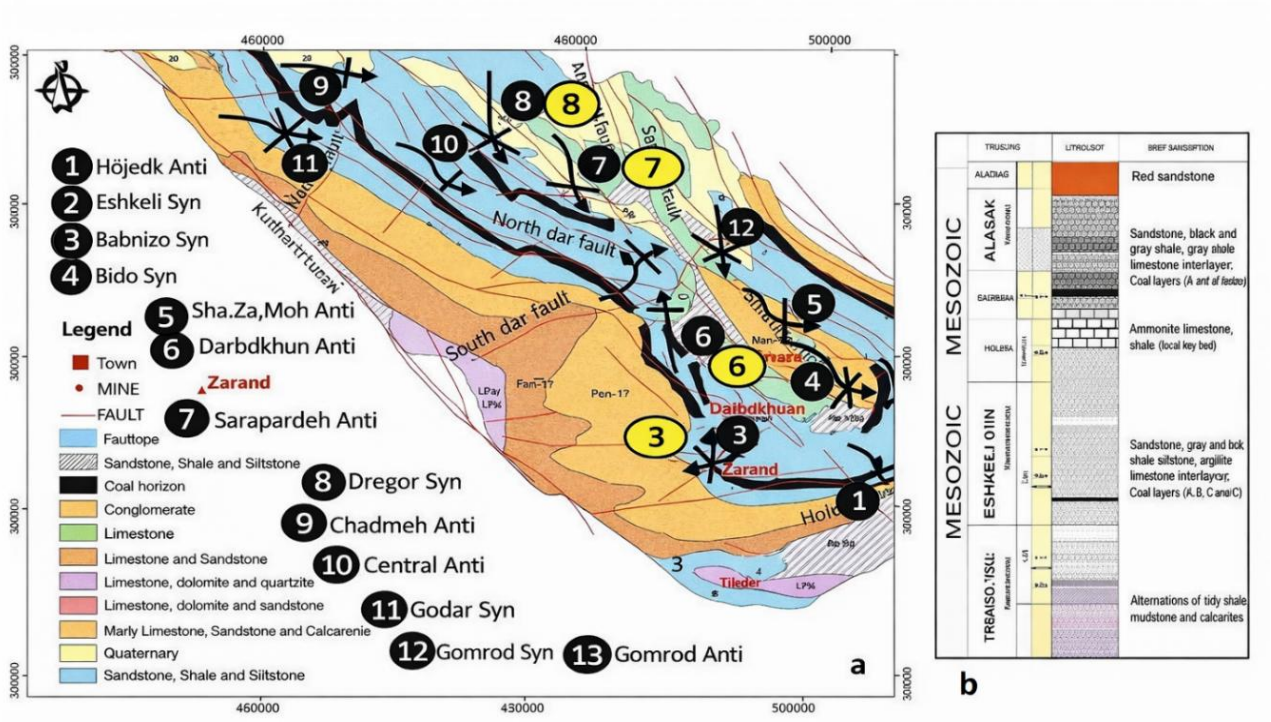

Figure 2. a) Geological map of the southern part of the Kerman coal basin; b) The stratigraphy of the Upper Triassic-Jurassic period and the sequence of coal units based on the division provided by the National Committee for Stratigraphy (Vahdati Daneshmand, 1995) and Technoexport Company (with slight modification from Amiri and Daftarian, 2015)

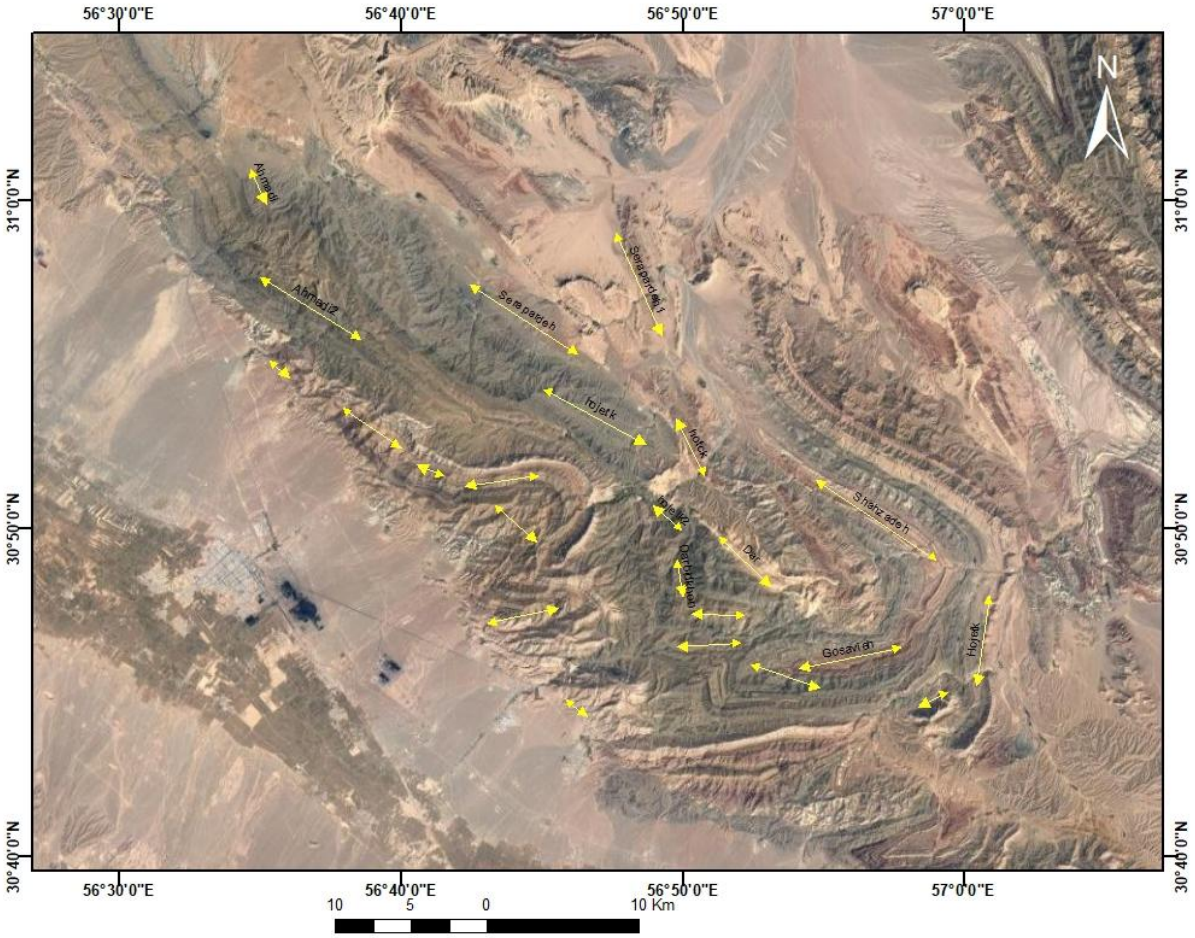

Figure 3. Satellite photo of the study area representing the axial effect of folds

10.57647/ijes.2025.16907

Table 1. Specifications of the folds in the study area

No.	Fold name	Fold length (Km)	Fold width (Km)	Average limb slope (°)	Average limb direction (°)	Limb direction
1	Hojadk Anticline*	6				
2	Eshkli Syncline	31	0.5	73/73	125/305	SW-NE
3	Beydo Syncline	40	3	65/36	24/195	SW-NE
4	Shahzadeh Mohammad Anticline	35	3.5-6	65/85	0/165	N-S
5	Babnizo Syncline	7.5	1-3.5	75/76	305/106	N-S
6	Darbidkhun Anticline	11	3	73/74	80/261	E-W
7	Dreger Syncline	30	1-1.5	64/70	92/271	N-S
8	Sarapardeh Anticline	30	5-Mar	32/86	134/315	N-S
9	Markazi Anticline	46	2-Jan	52/43	8/177	E-W
10	Gomroud Anticline	6	4-Feb	85/45	117/297	SW-NE
11	Gomroud Syncline	7.5	1-1.5	62/64	55/235	N-S
12	Chadmeh Anticline	8	5	65/73	109/298	N-S
13	Godar Syncline	43	1	79/73	0/110	E-W
14	Chevron Gosaviyeh Syncline	-	5-Nov	50/76	129/311	SW-NE
15	Hossein Abad Anticline	-	0.1	75/40	70/250	SW-NE
16	Babnizo Synclinirum	0.05	0.18	53/29	336/160	N-S
17	Darbidkhun concentric syncline	0.05	0.045	30/23	90/270	N-S
			0.045	23/30	6/181	N-S

3.1. Analyzing the closeure of folds

Based on the obtained information (angle between two limbs (i) and folding angle (∅)), the folds of the study area are divided into 4 main groups (Fig. 6):

A: Folds with i = 60° to 110° and ∅ = 120° to 70° are classified as Open folds.

B: Two folds (syncline x and syncline x) with ∅ < 60° and an i > 120° belong to the Gentle folds group.

C: Folds x and x with ∅ = 110 to 150° and i = 30 to 70° are Closed folds.

D: The reverse syncline with ∅ = 20 and i = 160° is classified as Tight (Table 1).

3.2. Analyzing the aspect ratio (p) of folds in the study area

The aspect ratio (p) is one of the geometric indicators of the folding style. This index is the ratio of the fold

10.57647/ijes.2025.16907

amplitude (A) to half the wavelength distance (M). With the above definition, this index can be determined only when the entire folded surface or layer is directly measurable or captured in a photo.
Nevertheless, in the study area, due to the extent and scale of the folds, the erosion of different parts of the folds, and the lack of access to the complete profile, it was not possible to measure the parameters required to calculate this index (i.e., p). Therefore, this index was calculated for all folds of the region using the graph of the relationship between the inter-dial angle (i) and the apparent ratio (p)

Table 2. Dimensions and characteristics calculated for the folds of the study area

No.	Fold name	Interlimb angle (i°)	Folding angle (θ°)	Axis coordinates	Axial plain
1	Hojadk Anticline*	40	140	4,289	118,66S
2	Eshkli Syncline	109	71	4,197	15,83E
3	Beydo Syncline	118	62	10,353	353,89E
4	Shahzadeh Mohammad Antiline	29	151	5,308	328,89S
5	Babnizo Syncline	32	147	2,80	80,88S
6	Darbidkhun Anticline	46	134	7,274	247,88N
7	Dreger Syncline	62	118	6,124.50	308,64N
8	Sarapardeh Anticline	86	94	5,183	183/85W
9	Markazi Anticline	60	120	0,295	297/67N
10	Gomroud Anticline	54	126	0.55	55,89S
11	Gomroud Syncline	54	126	9,112	293,83N
12	Chadmeh Anticline	80	100	52,124	321.77E
13	Godar Syncline	54	126	2,130	310,77N
14	Chevron Gosaviyeh Syncline	82	98	2,337	159,78W
15	Hossein Abad Anticline	65	115	5,70	70,70S
16	Babnizo Synclinirum	53	127	0,270	90,86S
17	Darbidkhun concentric syncline	53	127	1,3	183,87W

(Ghassemi et al., 2010). Fig. 7 illustrates the nomogram of the relationship between p and i. Also, the p-values are given in Table 1.
A: Most folds with a p = 0.25 to 0.63 are classified as Broad folds.
B: Babnizo and Darbidkhun synclines with p = 0.63 to 1.56 are Equant folds.
C: Shahzadeh Mohammad folds with p < 0.25 and p = 0.25 are Wide folds and placed between the Wide and Broad folds.
D: Darbidkhun syncline with a p = 2.33 (i.e., the highest p among the folds of the region) falls in the category of Short folds.

4. Shortening strain in the studied fols

Among the 17 folds examined in terms of closer degree, three syncline structures (i.e., Babnizo, Eshkli, and Dregor) and three anticline structures (i.e., Hojadk, Darbidkhun, and Sarapardeh) have economic coal reserves. These structures are located at six points of the study area as follows:

1. Hojadk Anticline; sandstone, shale, and argillite (Upper Triassic, Jurassic), coal deposit in the Hojadk Formation.

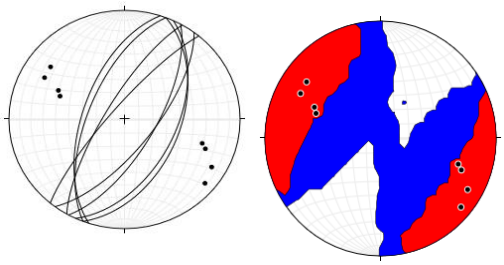

8 and β diagrams

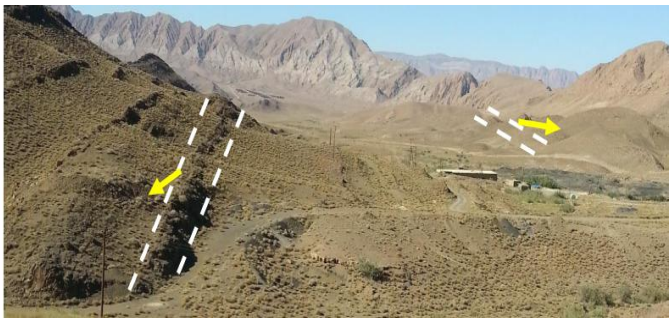

Field view: A minimum workable reserve of 15 million tons of coal

2. Sarapardeh Anticline: sandstone, argillite shale related to Jurassic, coal deposits of Sarapardeh, and Babshogun mines

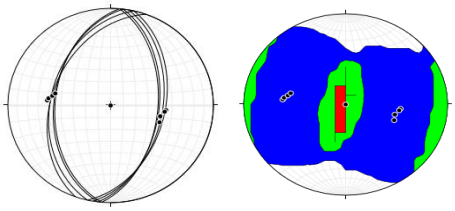

8 and β diagrams

Field view: A minimum workable reserve of 5 million tons of coal

3. Dregor Syncline: sandstone, shale, and coal beds related to Triassic and Jurassic

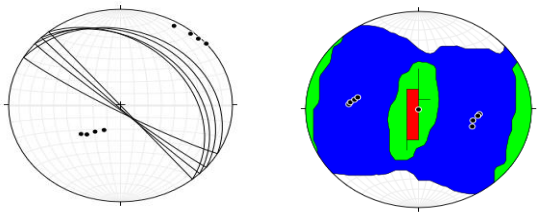

8 and β diagrams

Field view: At least 4 million tons of thermal coal

A: Field diagrams and photos

10.57647/ijes.2025.16907

4. Darbidkhun anticline, sandstone, argillite, and shale (Triassic and mainly Jurassic)

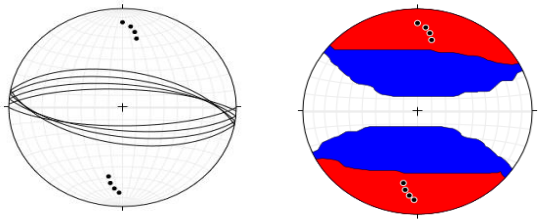

8 and β diagrams

Field view: At least 4 million tons of coal

5. Babnizo: Sandstone, argillite, and shale (Triassic and mainly Jurassic)

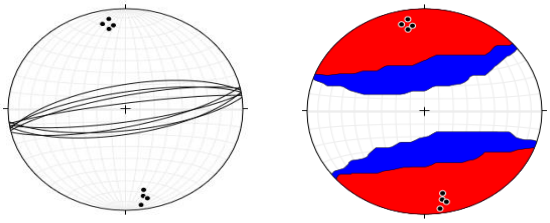

8 and β diagrams

Field view of the important center of Kerman coal reserves

6. Eshkli Syncline: sandstone, argillite, and alveolite (Triassic and Jurassic)

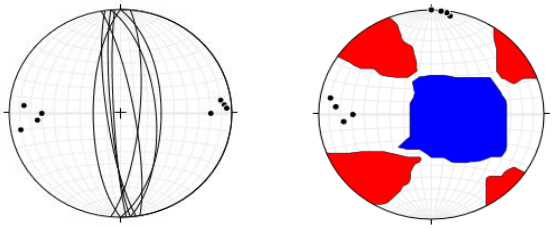

8 and β diagrams

Field view of the important center of Kerman coal reserves

4.1. Shortening calculations

To calculate the shortening degree, we need to have bluntness and aspect ratio:

Aspect Ratio: In the study area, the extent and scale of the folds, and the erosion of their different parts are not measurable indicators. Therefore, using the nomogram that relates the interlimb angle to the aspect ratio, the aspect ratio was calculated for all folds in the region (Table 3). Fig. 4 represents this nomogram (Ghassemi et al., 2010).

Bluntness (b): This index represents the relative bending of the fold at the hinge or closure of the fold. This index is defined based on the relationship between the bending radii in the closure place and the circle passing through the folds. Depending on the bending degree of each fold, b is defined as

$$b = \begin{cases} 2-{}^{r_c}/_{r_0} & r_c \geq r_0 \\ {}^{r_0}/_{r_c} & r_c \leq r_0 \end{cases}.$$

Based on their b-values, folds are divided into five categories: sharp, angular, semi-angular, semi-round, and

10.57647/ijes.2025.16907

round, and chamfered. Here, b varies between 0 (sharp folds) and 2 (blunt folds with two hinges). It is possible to obtain the numerical values of r0, rc, and b in two ways:
a: The direct method is employed for fine folds and folds that can be measured and imaged (macroscopic scale).
b: The indirect method through mathematical relationships is used for folds that cannot be measured directly.
In the study area, it was not possible to calculate b directly due to erosion, the covering of the folded valleys, the large-scale of the folds, and the lack of milestones in many folds. Therefore, by dividing the folds based on the folding angle (Ø) and aspect ratio (p) (Twiss 1998), b values were provided for the complete folds of the region (Fig. 4). In Fig. 4, the counterlines of Ø and p in different classifications of folds are drawn based on the angle between the two limbs. Based on these values, b was calculated with its results shown in Table 3.

According to Fig. 8 and Table 2, there are 4 fold groups based on the p classification:
Based on the obtained b values, the studied folds are classified into 6 categories (Fig. 8):
A: Hereditary anticline (b < 0.1) falls in the category of Sharp folds.
B: Both Babnizo and Darbidkhun synclines with b = 0.1 are placed on the border of Sharp and Angular folds.
C: The Eshkli anticline and Shahzadeh synclines fall in the category of Angular folds.
D: Anticline x is in the category of Semi-Rounded folds.
E: Syncline x with b = 0.4 lies at the border of Semi-angular categories and Semi-rounded.
F: The remaining eight folds with b = 0.2 to 0.4 are in the Semi-angular category.

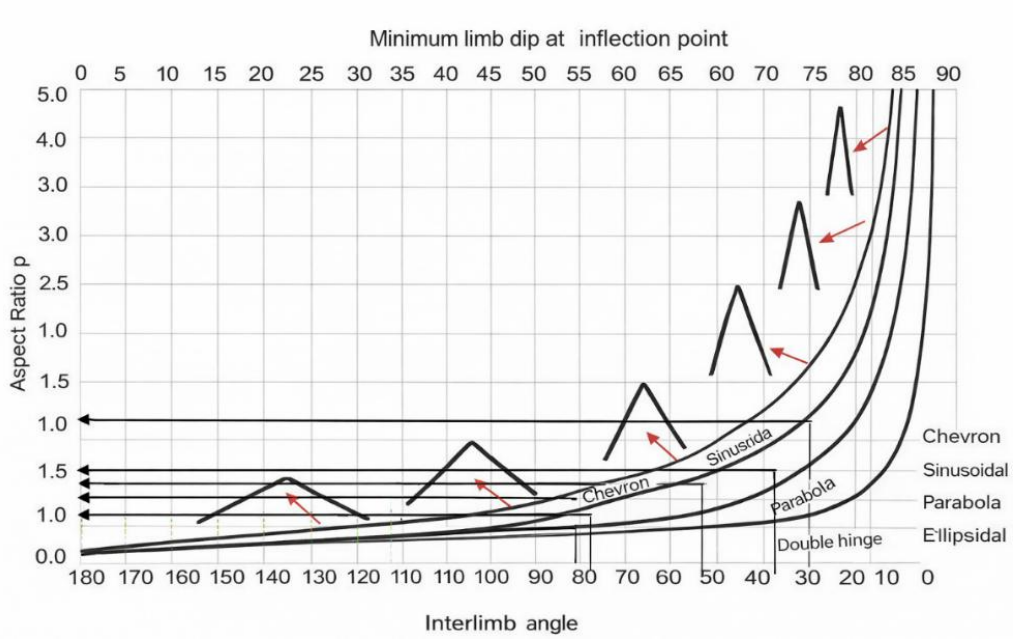

Figure 4. The diagram of bluntness (b) values in terms of interlimb angle (i) and aspect ratio (p); the values of p for the folds of the study area are obtained from the angle between their two limbs in Table 3

Table 3. Values of parameters log p, p, and i calculated for the selected folds of the study area

Fold Name	In. L.A (I)	Aspect Ratio (P)	Log(P)
Hojadk Anticline	40	0.86	-0. 6
Eshkli Syncline	71	0.6	-0.22
Babnizo Syncline	33	1.6	+0.2
Darbidkhun Anticline	46	1	0
Dregor Syncline	62	0.8	-0.09
Sarapardeh Anticline	86	0.56	-0.25

10.57647/ijes.2025.16907

5. Sharpness (b) calculations

As mentioned before, it is not possible to calculate b values directly due to erosion, the covering of the folded valleys, the large-scale nature of the folds, and the lack of milestones in many folds. Thus, values were provided for the complete folds of the region by dividing the folds based on the folding angle (Ø) and aspect ratio (p) (Twiss 1998), b (Fig. 5).

6. Analysis of the folding-induced shortening

In continental regions, intracontinental shortening in fold-and-thrust belts is often the most obvious manifestation of shortening. In these areas, shortening begins with the thickening of sediments and the folding of rock units from the sedimentary basin, with different patterns. Next, it proceeds and evolves with the progression of deformation, fold compression, and the formation of thrust and dependent faults.

Thickening and spalling of thrusts are the advanced stages of this type of deformation. At each stage of this progressive metamorphism, the development level of the folded structures is less severe than that of the other folds. The shortening of a fold using the amount and degree of shortening (interlimb angle), fold sharpness (b), i.e., the ratio of the height to the width of the fold, and the aspect ratio (P) (the ratio of the width of the fold (A) to the half wavelength distance (A)) can be estimated and calculated. In this research, a shortening study was performed using the Fabric8 software. Fig. 6 presents the methodology for reducing the calculation time, and Table 5 lists the resulting values.

The results show that the highest shortening rate of folds is 70% for the Babnizo syncline, and the lowest is 42% for the Eshkli syncline. Fig. 7 shows the two-dimensional surface strain ellipses calculated for each fold in the study area based on Fig. 6 and Table 5.

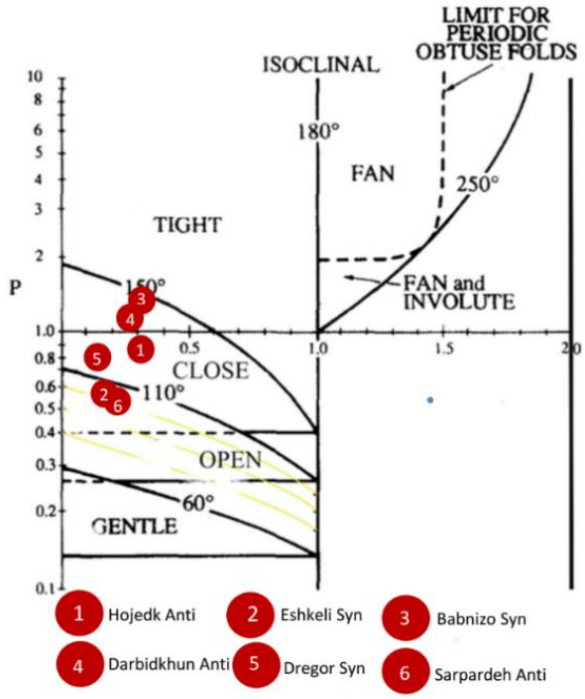

Figure 5. Ø Isocounters separating the folds based on their closure degree. The b values can be calculated according to the Ø angles for folds with different classifications. The image was adapted from Twiss (1988)

Table 4. Calculated values for the bluntness index for folds of the region

Fold Name	Bluntness (b)
Hojadk Anticline	0.31
Eshkli Syncline	0.2
Babnizo Syncline	0.31
Darbidkhun Anticline	0.3
Dregor Syncline	0.17
Sarapardeh Anticline	0.2

10.57647/ijes.2025.16907

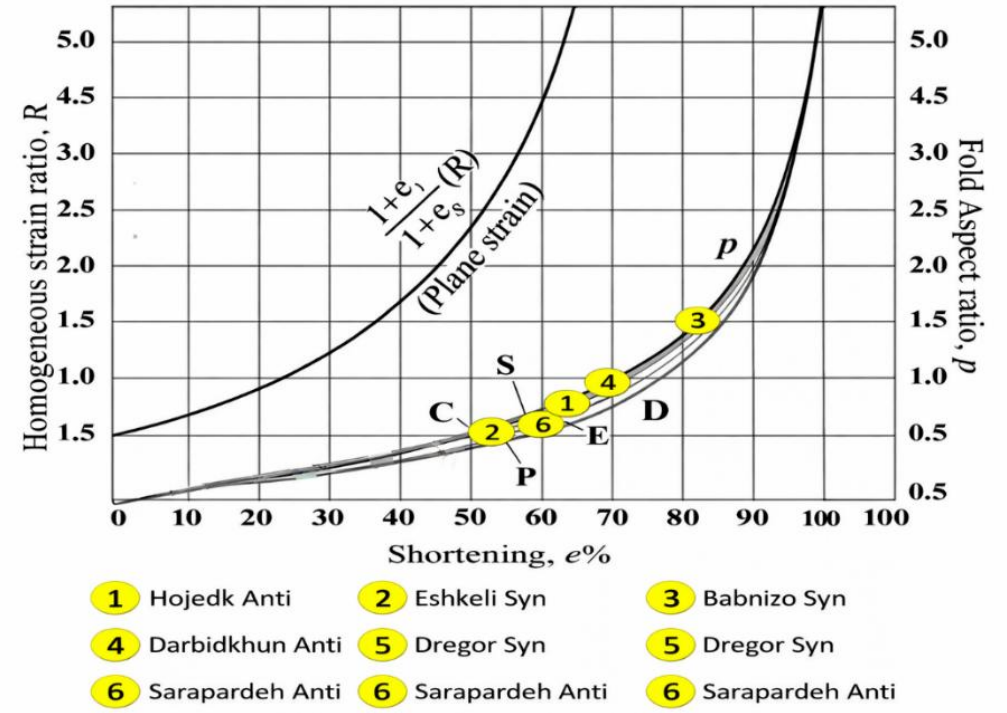

Figure 6. The values of shortening coordinates (e%) and the homogeneous strain ratio (R); note that there is a maximum amount of shortening for different fold shapes, the P-ratios of which are all less than 0.5 (Types of folds: C: Chevron, S: Sinusoidal, P: Parabolic, E: Elliptical, and D: Double)

Table 5. Calculated shortening for the folds of the study area

Name	Shortening (e%)
Sarapardeh Anticline	51%
Dregor Syncline	56%
Eshkli Syncline	42%
Darbidkhun Anticline	59%
Hojadk Anticline	51%
Babnizo Syncline	70%

7. Discussion

This research paper, therefore, investigates tectonic deformation processes characterized by folding and faulting that defined the southern part of the Kerman coal field in central Iran, thereby explaining their implications for the tectonic history. This critical analysis will help review the broader geological settings, including how compressive and extensional stresses have shaped the landscape, the relative timing of fault and fold formations, and the implications for regional tectonics. The same processes could be adapted for further geological studies and resource management in the area. Folding and faulting in the southern Kerman-Behabad coal field mark a complex tectonic history influenced by compressive and extensional stresses, similar to the geological dynamics observed in neighboring regions such as the Yazd and Tabas areas. Folds in the Kerman-Behabad region can be divided into four major types based on variations in their interlimb and folding angles, reflecting different tectonic forces. This classification also aligns with findings in the Yazd region, where such fold structures have been documented as evidence of regional consistency in tectonic activities (Ameri et al., 2022; Mansoui et al., 2020).

- Open folds: i=60° to 110° and θ=120° to 70°
- Mild folds: i>120° and θ<60°
- Closed folds: i=30 to 70° and θ=110 to 150°
- Tight folds: i=160° and θ=20°

In the Kerman-Behabad area, most folds have a pp ratio of 0.25-0.63, suggesting the dominance of broad folds in the area. This result is confirmed by observations in the Tabas region, which also has wide folds, indicating a similar response to tectonic forces across these regions. Various Kuhbanan and Lekarkoh faults, which had an intense impact on the structural development of the Kerman-Behabad coal field, predate folding events (Ameri et al., 2022). The study conducted in the Yazd region indicated that the same type of faulting, though important for the geometrical development of the geological skeleton, was active before folding. The variability in shortening rates between 42% and 70% indicates heterogeneous deformation; accordingly, it supports the observation of the Tabas region reported by Mansouri et al. (2020). This level of variability was also documented further north in the Tabas region, which has been similarly interpreted in terms of variable shortening rates under local tectonic conditions. Other types of non-tectonic folding, such as gravity and expansion folds, may also need to be considered, as their presence has recently been reported in the Yazd region by Ameri et al. (2022). Most of these features have not been studied in detail in the Kerman-Behabad area, whereas their identification in the Yazd region may suggest a wider formation deserving of attention. Meanwhile, although the record of tectonic history is remarkably clear in the Kerman-Behabad region, the presence of non-tectonic features may indicate that complex interactions among geological processes remain incompletely understood. This comparative approach enhances understanding of tectonic development in central Iran and establishes a broader framework for future studies.

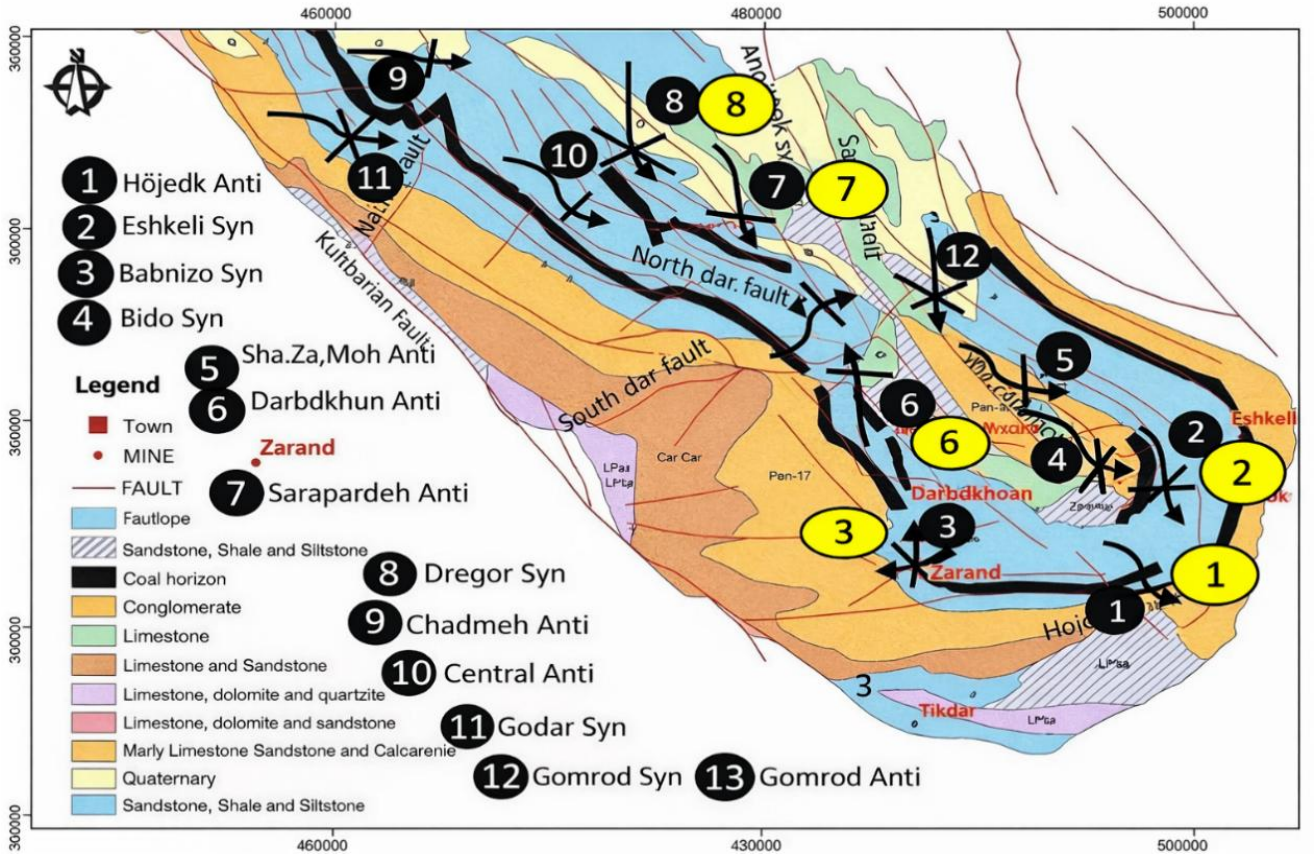

Figure 7. Spatial representation of shortening strain ellipses on the geological map of the southern part of the Kerman coal basin

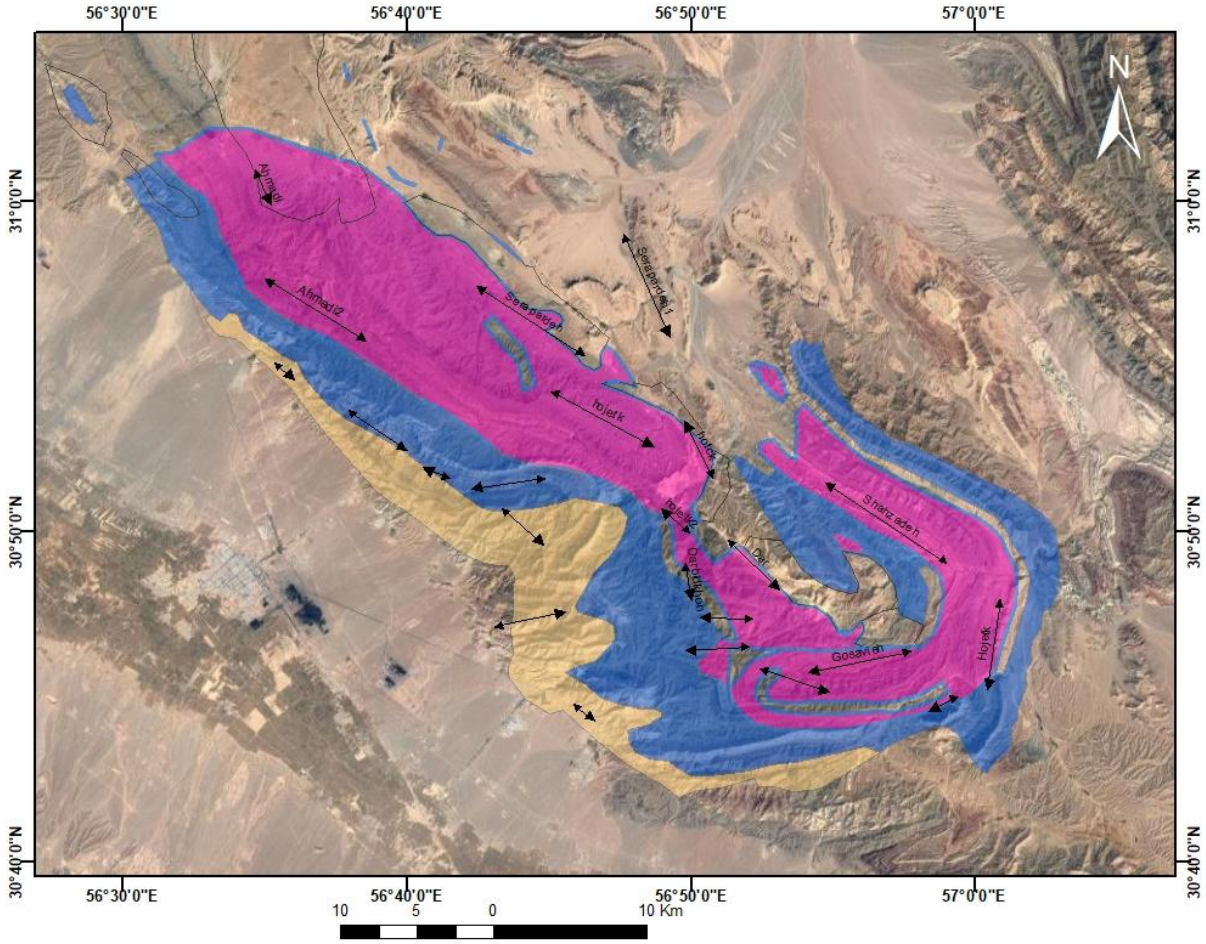

Figure 8. The satellite image (Hotbird-Google Earth) of the study area and the position of the folds and their degree of narrowing, separated by colors, are displayed on it (refer to the text for more explanation)

8. Conclusion

The investigation of folding in the southern Kerman-Behabad coal field provides essential information on the tectonic and deformational history of the region. Compressional folding is interpreted due to the Alpine tectonic events, and the maximum shortening on the Babnizo fold is about 70%, while the Eshkli syncline shows a minimum shortening of 42%. The research highlighted the successive development of both ductile and brittle structures; therefore, the majority of the faults in the region formed after folding, except for Kuhbanan and Lekarkoh, which contributed to shaping the area's general structure before folding. The folding types that are open, gentle, closed, and tight folds support the complexity of the tectonic environment. Hence, the results confirm that compressive interactions and extensional stresses are responsible for the deformation in the investigated area. This work generally contributes to a better understanding of the geological processes involved in this tectonically active region. According to Fig. 8, the folds of Darbidkhun, Babnizo, Hojedk, and Shahzadeh Mohammad are compressed from the sides toward the center. Also, the angles between the two limbs of the folds are wider at the ends of the Darbidkhun syncline, suggesting the formation of new folds with the same mechanism at both ends. The above folds provide a complete representation of a folded belt, indicating the formation of folds from the initial stages to compression and return in a time sequence.

Authors Contribution
All the authors have participated sufficiently in the intellectual content, conception, and design of this work or the analysis and interpretation of the data (when applicable), as well as the writing of the manuscript.

Availability of data and materials
The data that support the findings of this study are available from the corresponding author upon reasonable request.

Conflict of interest
The author states that there is no conflict of interest.

10.57647/ijes.2025.16907

References

Aghanabati, A. 2004. Geology of Iran [in Persian]. Geological Survey of Iran, Tehran, 586 pp.

Ait Haddou, M., Bouchriti, Y., Belkacim, S., Yazdi, A. and Kabbachi, B., 2025. Late Carboniferous Paleoflora of El Menizla Formation (Argana Corridor, Morocco): Implications for Geotourism and Geoconservation, *Geoheritage*, 17(4):151.
DOI: https://doi.org/10.1007/s12371-025-01202-5

Allen, M.B., Ghassemi, M.R., Shahrabi, M. and Qorashi, M. 2003. Accommodation of late Cenozoic oblique shortening in the Alborz range, northern Iran. *Journal of Structural Geology*, 25, pp. 659–672.
DOI: https://doi.org/10.1016/S0191-8141(02)00064-0

Ameri, S., Solgi, A., Sorbi, A. and Farrokhnia, A. 2022. Identification of faults with seismic hazard potential based on morphotectonic analysis, Kerman city (Southeastern Iran). *Earth Sciences Research Journal*, 26(1), pp. 23–38.
DOI: https://doi.org/10.15446/esrj.v26n1.83186

Arjmandzadeh, R., Rashvanlou, V.S., Dabiri, R. and Almasi, A. 2017. Satellite thermal surveys to detecting hidden active faults and fault termination: Case study of Quchan fault, NE Iran. *Iranian Journal of Earth Sciences*, 9(1), pp. 39–47.

Berberian, M., Jackson, J.A., Fielding, E., Parsons, B., Priestley, K., Qorashi, M., Talebian, M., Walker, R., Wright, T.J. and Baker, C. 2001. The 1998 March Fandoqa earthquake (Mw 6.6) in Kerman province, southeast Iran; re-rupture of the 1981 Sirch earthquake fault, triggering of slip on adjacent thrusts and the active tectonics of the Gowk fault zone. *Geophysical Journal International*, 146, pp. 371–398.
DOI: https://doi.org/10.1046/j.1365-246x.2001.01459.x

Berberian, M., Jackson, J.A., Qorashi, M., Khatib, M.M., Priestley, K., Talebian, M. and Ashtiani, M. 1999. The 1997 May 10 Zirkuh (Qa'enat) earthquake (M 7.2): faulting along the Sistan suture zone of eastern Iran. *Geophysical Journal International*, 136, pp. 671–694.
DOI: https://doi.org/10.1046/j.1365-246x.1999.00762.x

Berberian, M. and King, G.C.P. 1981. Towards a paleogeography and tectonic evolution of Iran. *Canadian Journal of Earth Sciences*, 18, pp. 210–265.
DOI: https://doi.org/10.1139/e81-019

Berberian, M. and Yeats, R.S. 1999. Patterns of historical earthquake rupture in the Iranian plateau. *Bulletin of the Seismological Society of America*, 89, pp. 120–139.
DOI: https://doi.org/10.1785/BSSA0890010120

Camp, V. and Griffis, R. 1982. Character, genesis and tectonic setting of igneous rocks in the Sistan suture zone, eastern Iran. *Lithos*, 15, pp. 221–239.
DOI: https://doi.org/10.1016/0024-4937(82)90014-7

Dabiri, R., Adli, F. and Javanbakht, M. 2017. The environmental impacts of Aghdarband coal mine: Pollution by heavy metals. *Geopersia*, 7(2), pp. 313–323.
DOI: https://doi.org/10.22059/geope.2017.229525.648308

Ezati, M. and Gholami, E. 2022. Neotectonics of the Central Kopeh Dagh drainage basins, NE Iran. *Arabian Journal of Geosciences*, 15, 992.
DOI: https://doi.org/10.1007/s12517-022-10280-6

Fleuty, M.J. 1964. The description of folds. *Proceedings of the Geologists' Association*, 75(4), pp. 461–492.
DOI: https://doi.org/10.1016/S0016-7878(64)80023-7

Ghanbarian, M.A. and Derakhshani, R. 2022. The folds and faults kinematic association in Zagros. *Scientific Reports*, 12, 8350.
DOI: https://doi.org/10.1038/s41598-022-12337-8

GhasemShirazi, B., Bakhshandeh, L. and Yazdi, A. 2014. Biozonation and paleobathymetry based on foraminifera of Upper Cretaceous deposits in Central Iran basins (Isfahan, Baharestan section). *Open Journal of Geology*, 4(8), pp. 343–353.
DOI: http://dx.doi.org/10.4236/ojg.2014.48026

Ghassemi, M.R., Schmalholz, S.M. and Ghassemi, A. 2010. Kinematics of constant arc length folding for different fold shapes. *Journal of Structural Geology*, 32, pp. 755–765.
DOI: https://doi.org/10.1016/j.jsg.2010.05.002

Javadi, H.R., Ghassemi, M.R., Shahpasandzadeh, M., Guest, B., Ashtiani, M.E., Yassaghi, A. and Kouhpeyma, M. 2013. History of faulting on the Doruneh Fault System: Implications for the kinematic changes of the Central Iranian Microplate. *Geological Magazine*, 150(4), pp. 651–672.
DOI: https://doi.org/10.1017/S0016756812000751

Jentzer, M., Whitechurch, H., Agard, P., Ulrich, M., Caron, B., Zarrinkoub, M.H., Kohansal, R., Miguet, L., Omrani, J. and Fournier, M. 2020. Late Cretaceous calc-alkaline and adakitic magmatism in the Sistan suture zone (Eastern Iran): Implications for subduction polarity and regional tectonics. *Journal of Asian Earth Sciences*, 204, 104588.
DOI: https://doi.org/10.1016/j.jseaes.2020.104588

Mansouri, H., Shafiei Bafti, A. and Pourkermani, M. 2020. The power law scaling, geometric and kinematic characteristic of faults in the northern part of the Kerman Coal Province (KCP), *Iran. Iranian Journal of Earth Sciences*, 12(2), pp. 124–132.

McCall, G.J.H. 1996. The inner Mesozoic to Eocene ocean of south and central Iran and associated microcontinents. *Geotectonics*, 29, pp. 490–499.

Rashidi, A. and Derakhshani, R. 2022. Strain and moment-rates from GPS and seismological data in Northern Iran: Implications for an evaluation of stress trajectories and probabilistic fault rupture hazard. *Remote Sensing*, 14, 2219.
DOI: https://doi.org/10.3390/rs14092219

Rashidi, A., Khatib, M.M. and Derakhshani, R. 2022. Structural characteristics and formation mechanism of the earth fissures as a geohazard in Birjand, Iran. *Applied Sciences*, 12, 4144.
DOI: https://doi.org/10.3390/app12094144

Saccani, E., Delavari, M., Dolati, A., Pandolfi, L., Barbero, E., Brombin, V. and Marroni, M. 2022. Geochemistry of volcanic rocks and dykes from the Remeshk–Mokhtarabad and Fannuj–Maskutan ophiolites (Makran Accretionary Prism, SE Iran): New constraints for magma generation in the Middle East Neo-Tethys. *Geosystems and Geoenvironment*, 100140.
DOI: https://doi.org/10.1016/j.geogeo.2022.100140

Sella, G.F., Dixon, T.H. and Mao, A. 2002. REVEL: A model for recent plate velocities from space geodesy. *Journal of Geophysical Research*, 107(B4), 2081.

Shafii, B.A. and Amiri, A. 1998. Investigating and evaluating gypsum reserves in Zarand region. Research project, *Islamic Azad University, Zarand Branch*, 103 pp.

Tadayon, M., Rossetti, F., Zattin, M., Nozaem, R., Calzolari, G., Madanipour, S. and Salvini, F. 2017. The post-Eocene evolution of the Doruneh Fault region (Central Iran): The intraplate response to the reorganization of the Arabia–Eurasia collision zone. *Tectonics*, 36, pp. 3038–3064.
DOI: https://doi.org/10.1002/2017TC004595

Technoexport (Soviet Union). 1969. Geological map of the Kerman coal deposits. *National Iranian Steel Company*, Contract No. 1466.

Tirrul, R., Bell, I., Griffis, R. and Camp, V. 1983. The Sistan suture zone of eastern Iran. *Geological Society of America Bulletin*, 94(1), pp. 134–150.
DOI: https://doi.org/10.1130/00167606(1983)94<134:TSSZOE>2.0.CO;2

Twiss, R.J. 1988. Description and classification of folds in single surfaces. *Journal of Structural Geology*, 10, pp. 607–623. DOI: https://doi.org/10.1016/0191-8141(88)90027-2

Twiss, R.J. and Moores, E. 2007. Structural Geology, 2nd ed. New York: *W.H. Freeman and Company*, 736 pp.

Vahdati Daneshmand, F. and Nadim, H. 1995. Geological map of Zarand, scale 1:100,000. *Geological Survey of Iran, Tehran*.

Vernant, P., Nilforoushan, F., Hatzfeld, D., Abbassi, M., Vigny, C., Masson, F., Nankali, H., Martinod, J., Ashtiani, A. and Bayer, R. 2004. Present-day crustal deformation and plate kinematics in the Middle East constrained by GPS measurements in Iran and northern Oman. *Geophysical Journal International*, 157, pp. 381–398. DOI: https://doi.org/10.1111/j.1365-246X.2004.02222.x